

Chirp modulation stimulated Raman scattering microscopy: supplement

ADRIAN F. PEGORARO^{1,2,6},  AND ALBERT STOLOW^{2,3,4,5,7}

¹*Metrology Research Centre, National Research Council of Canada, 100 Sussex Drive, Ottawa, ON, K1A 0R6, Canada*

²*Department of Physics, University of Ottawa, Ottawa ON, K1N 6N5, Canada*

³*Department of Chemistry, University of Ottawa, Ottawa ON, K1N 6N5, Canada*

⁴*Max-Planck-Ottawa Centre for Extreme and Quantum Photonics, Ottawa ON, K1N 6N5, Canada*

⁵*Quantum and Nanotechnologies Research Centre, National Research Council of Canada, 100 Sussex Drive, Ottawa, ON, K1A 0R6, Canada*

⁶*adrian.pegoraro@nrc-cnrc.gc.ca*

⁷*astolow@uottawa.ca*

This supplement published with Optica Publishing Group on 13 August 2024 by The Authors under the terms of the [Creative Commons Attribution 4.0 License](https://creativecommons.org/licenses/by/4.0/) in the format provided by the authors and unedited. Further distribution of this work must maintain attribution to the author(s) and the published article's title, journal citation, and DOI.

Supplement DOI: <https://doi.org/10.6084/m9.figshare.26504461>

Parent Article DOI: <https://doi.org/10.1364/OE.531274>

Chirp modulation stimulated Raman scattering microscopy: Supplementary Material

1. Analytics

The third-order Raman polarization is described analytically using well-known approaches [1–3], starting from:

$$P^{(3)}(\omega_{CRM}) = \int_{-\infty}^{\infty} d\omega_P \int_{-\infty}^{\infty} d\omega_S \int_{-\infty}^{\infty} d\omega_{Pr} \chi^{(3)}(-\omega_{CRM}, \omega_P, \omega_S, \omega_{Pr}) E_P(\omega_P) E_S(\omega_S) E_{Pr}(\omega_{Pr}) \delta(\omega_{CRM} - \omega_P + \omega_S - \omega_{Pr}) \quad (S1)$$

where $P^{(3)}(\omega_{CRM})$ is the frequency component of the nonlinear polarization at ω_{CRM} , $E_P(\omega_P)$ denotes the pump field, $E_S(\omega_S)$ denotes the Stokes field and $E_{Pr}(\omega_{Pr})$ is the probe field which, for SRS, is simply the complex conjugate of the Stokes. The delta function ensures the resonance condition. $\chi^{(3)}$ is the third order susceptibility which we assume here takes the simple form:

$$\frac{A_R}{\Omega_R - (\omega_P - \omega_S) - i\Gamma} + \chi_{NR} \quad (S2)$$

where A_R is the relative strength of the Raman oscillator, Ω_R is central vibrational frequency and Γ determines the Raman linewidth. χ_{NR} denotes the contributions of all non-Raman process and is assumed to be Raman frequency independent. Each electric field is represented as a chirped Gaussian:

$$E_i(\omega_i) = \frac{E_{0i}}{\sqrt{\Delta_i}} \exp\left(\frac{-(2 \ln 2)(\omega_i - \Omega_i)^2}{\Delta_i^2} (1 + iqa)\right) \quad (S3)$$

where E_{0i} is the strength of the electric field, Ω_i is the central frequency, a is the magnitude of the chirp (quadratic phase), q is the sign (± 1) of the chirp and Δ_i is the spectral bandwidth of the pulse. For simplicity, all pulses are assumed to have the same electric field strength E_0 , chirp magnitude a , and bandwidth Δ . Additionally, the Stokes and probe beams are assumed to have the same center frequency Ω_S . Substituting (S2) and (S3) into (S1) the expression for the polarization becomes:

$$P^{(3)}(\omega_{CRM}) = \int_{-\infty}^{\infty} d\omega_P \int_{-\infty}^{\infty} d\omega_S \int_{-\infty}^{\infty} d\omega_{Pr} \left(\frac{A_R}{\Omega_R - (\omega_P - \omega_S) - i\Gamma} + \chi_{NR} \right) \frac{E_0^3}{\sqrt{\Delta^3}} \exp\left(\frac{-(2 \ln 2)(\omega_P - \Omega_P)^2}{\Delta^2} (1 + ia)\right) \exp\left(\frac{-(2 \ln 2)(\omega_S - \Omega_S)^2}{\Delta^2} (1 - iqa)\right) \exp\left(\frac{-(2 \ln 2)(\omega_{Pr} - \Omega_S)^2}{\Delta^2} (1 + iqa)\right) * \delta(\omega_{CRM} - \omega_P + \omega_S - \omega_{Pr}) \quad (S4)$$

where Ω_P is the pump center frequency. Here we have assumed the pump is always positively chirped whereas the Stokes/probe beams are positively chirped with $q = +1$ for the co-chirped case and negatively chirped with $q = -1$ for the contra-chirped case. Simplifying the above expression for the co-chirped case ($q = +1$) we find that:

$$P_{co}^{(3)}(\omega_{CRM} + \Omega_P) \propto A \exp\left(-\left(\frac{1+a^2}{3-ia}\right) \frac{2 \ln 2}{\Delta^2} \omega_{CRM}^2\right) * \int \frac{\exp\left(-\left(\frac{3+2ia+a^2}{2}\right) \frac{2 \ln 2}{\Delta^2} \left(\omega - \frac{2}{3-ia} \omega_{CRM}\right)^2\right)}{\Omega_R + \Omega_S - \Omega_P - \omega - i\Gamma} d\omega \quad (S5)$$

whereas for the contra-chirped case ($q = -1$) it becomes:

$$P_{Contra}^{(3)}(\omega_{CRM} + \Omega_p) \propto \frac{A}{\sqrt{1+ia}} \exp\left(-\left(\frac{1+a^2}{3-ia}\right) \frac{2 \ln 2}{\Delta^2} \omega_{CRM}^2\right) * \int \frac{\exp\left(-\left(\frac{3-ia}{2}\right) \frac{2 \ln 2}{\Delta^2} \left(\omega - \frac{2-2ia}{3-ia} \omega_{CRM}\right)^2\right)}{\Omega_R + \Omega_S - \Omega_P - \omega - i\Gamma} d\omega \quad (S6)$$

In the limit $a \rightarrow 0$, both pulses become transform-limited and Eq. (S5) and (S6) are identical. In both co- and contra-chirped cases, $P^{(3)}$ is the convolution of a Lorentzian Raman resonance with an effective (i.e. chirp dependent) Gaussian excitation spectrum (i.e. the Pump-Stokes difference-frequency spectrum, which is chirp-dependent): this convolution is a Voigt lineshape.

For non-Raman terms (i.e. flat spectral response), the integrals simplify to:

$$P_{Non-Raman}^{(3)}(\omega_{CRM} + \Omega_p) \propto \frac{A_{NR}}{\sqrt{3+2ia+a^2}} \exp\left(-\left(\frac{1+a^2}{3-ia}\right) \frac{2 \ln 2}{\Delta^2} \omega_{CRM}^2\right) \quad (S7)$$

for both the co- and contra-chirped cases. Importantly, the equality of these two cases is why CM subtracts all non-Raman signals.

2. Simulations

The analytic expressions for the third order polarization indicate that the CM-SRS signal scales linearly with the Raman oscillator strength; however, this does not directly determine the Raman spectral line shape because, in CM-SRS, the experimentally measured spectrum is the interference signal between the generated polarization and the pump. To simulate the CM-SRS lineshape, it is convenient to use noise-free data in order to clearly illustrate the deconvolution procedure. To this end, we numerically calculated the Raman response for co-AM-SRS and contra-AM-SRS. Absenting low-frequency noise in the numerical calculations, this directly yields the CM-SRS response: co-AM-SRS minus contra-AM-SRS. We illustrate in Fig. S1 the case for two close-lying Raman resonances. As shown in Fig. S1(a), the numerical simulations show the well-known result that the co-AM-SRS spectrum is distributive and linear in the Raman response. For co-AM-SRS, the intensity spectra from two close-lying Raman resonances are calculated when they are isolated (blue, orange) and when they are both present simultaneously (grey). Co-adding the independently calculated responses results in a spectrum that is essentially indistinguishable from the full spectral response and is not shown here. Similarly, the CM-SRS spectrum is distributive and linear in the Raman response, as shown in Fig. S1(b). To further emphasize the distributive and linear aspects of the AM-SRS and CM-SRS responses, we show in Fig. S1(c) the percentage difference between (i) calculating the individual Raman spectra separately and then co-adding (i.e. blue + orange lines) versus (ii) the Raman spectra of the two-resonance system (i.e. grey lines). The residuals in both AM-SRS and CM-SRS are small, statistically distributed and attributable here to residual numerical noise. The distributed and linear nature of CM-SRS is important, as it guarantees the linearity of the deconvolution process.

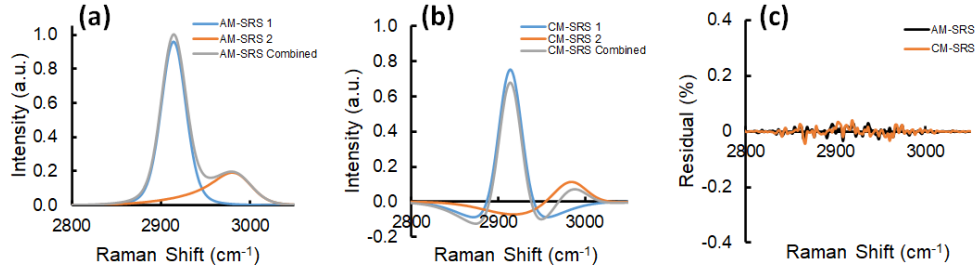


Fig. S1: Distributive and linear properties of AM- and CM-SRS. (a) AM-SRS spectra are calculated for two independent Raman resonances (blue and orange lines) and for both resonances being present simultaneously (grey line). (b) CM-SRS spectra are calculated for two independent Raman resonances (blue and orange lines) and for both resonances being present simultaneously (grey line). (c) Difference between co-adding independently calculated Raman responses (i.e. blue + orange) versus the full Raman response (i.e. grey line) for AM-SRS (black line) and CM-SRS (orange line).

For completeness, we also calculated the FM-CARS and CM-CARS responses under the assumption of a strong non-resonant background. FM-CARS [4] is typically dominated by the heterodyne response in the system and may be calculated by taking the difference between spectra with and without a Raman resonant contribution (i.e. resonant plus non-resonant versus non-resonant background only). CM-CARS is simply the extension of the CM-SRS concept to the CARS process: it is the difference between the co-chirped CARS and contra-chirped CARS signals. By analogy with CM-SRS, it should be possible to reduce the contribution of the non-Raman background terms to the measured Raman spectra and, therefore, CM-CARS is currently under investigation in our laboratory. In these simulations, FM-CARS and CM-CARS are each linear in Raman response, since the heterodyne term is large compared to the homodyne resonant term (see Figs. S2(a), S2(b)). However, as expected, the small residuals (Fig. S2(c), calculated analogously to Fig. S1(c)) are no longer statistically distributed but are due to the well-known coherent interferences inherent to the CARS process. While beyond the scope of the current work, existing techniques for recovering linear Raman spectra from CARS spectra [5,6] can be equally applied to CM-CARS.

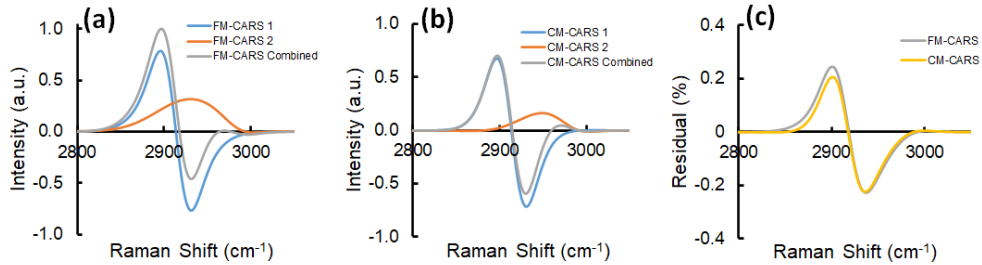


Fig. S2: Lack of distributive and linear properties of FM- and CM-CARS. (a) FM-CARS spectra are calculated for two independent Raman resonances (blue and orange lines) and for both resonances being present simultaneously (grey line). (b) CM-CARS spectra are calculated for two independent Raman resonances (blue and orange lines) and for both resonances being present simultaneously (grey line). (c) Difference between co-adding independently calculated Raman responses (i.e. blue + orange) versus the full Raman response (i.e. grey line) for FM-CARS (black line) and CM-CARS (orange line).

3. Experimental Results

A potential source of concern in any experimental realization of CM-SRS is the ability to match the magnitudes of the quadratic phase terms for the co- and contra-chirped beams; the differing optical paths and methods of chirp manipulation (stretcher versus compressor) result in beams with potentially mismatched higher-order (i.e. beyond quadratic) phases. The inability to correct the higher-order phases without making use of spatial light modulators is known to limit the achievable spectral resolution in spectral focusing SRS [7]. However, there is an important difference between Raman resonant and non-Raman signals. In Raman resonant processes, the dominant second order phase terms are set equal and subtracted such that higher-order phase terms are the residual contributors to the temporal profile of the generated third-order polarizability, determining the Raman spectral resolution. In non-Raman processes such as TPA and XPM, the temporal profile is determined overwhelmingly by the second order phase terms (i.e. the linear chirp). Given the dominance of the second order phase term in spectral focusing SRS, we expect that the small effects of nonideal and/or higher-order phases to be minimal with respect to the removal of non-Raman terms. To confirm this, we measured

the cross-correlation, using non-degenerate two-photon excited fluorescence (TPEF) in fluorescein, of each of the co- and contra-chirped beams with the pump, shown in Fig. S3. Importantly, we find that these are practically identical. Indeed, if we perform a CM measurement using TPEF detection, we eliminate this non-Raman response, confirming our expectation that CM efficiently removes non-Raman responses even with non-zero higher-order phases remaining uncorrected.

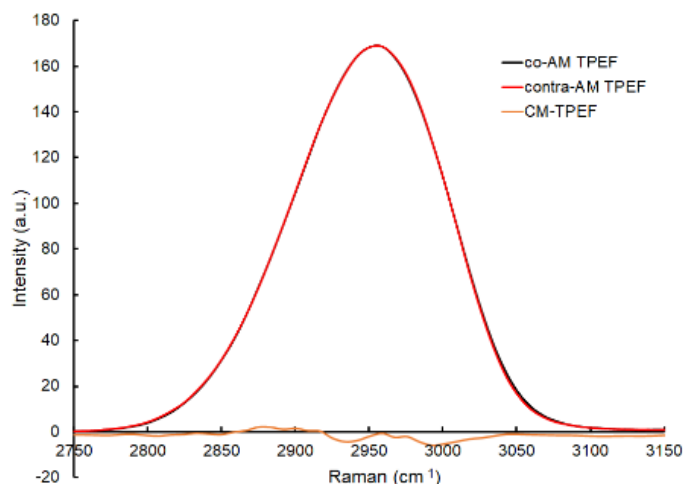


Fig. S3: Non-degenerate TPEF. Using a fluorescein solution, the cross-correlation of the pump (800 nm) with the co-chirped AM beam (black line) and contra-chirped AM beam (red line) were independently recorded. When both beams are present simultaneously in a CM-type measurement geometry, the response is nulled (orange line).

In AM-SRS, non-Raman responses can, in some samples, overwhelm the desired Raman-resonant signals, obviating chemical-specific contrast in imaging. In CM-SRS, these non-Raman responses are effectively removed but present unusual Raman lineshapes. However, as demonstrated above and in the main text, the CM-SRS spectrum is both distributive and linear with respect to the individual Raman resonances comprising the spectrum. Therefore, the CM-SRS spectrum can be deconvolved to yield a ‘standard’ Raman spectrum: specifically, the deconvolved CM-SRS spectrum is equivalent to the AM-SRS spectrum in the absence of all non-Raman backgrounds. While any compound with a sufficiently strong Raman response in the spectral region of interest can be used to determine the instrument response function of the microscope needed to perform the deconvolution, we typically use acetamidophenol, a known Raman standard in the fingerprint region [8].

In the main text, we highlighted two very challenging (i.e. strong non-Raman backgrounds) samples where CM-SRS demonstrably offers significant advantages in terms of chemical-specific contrast. In Fig. 4(a) of the main text, we showed that CM-SRS distinguishes different types of carotenoids in sweet potato, based on their individual Raman signatures. To recover the CM-SRS spectra, masks were defined based on image intensity at 1150 and 1520 cm^{-1} and the spectra reported in Fig. 4 of the main text were averaged over all masked pixels. Using the same masks defined for CM-SRS, we similarly determined the AM-SRS ‘spectra’ of the same materials, shown (magenta, cyan) in Fig. S4(b). The AM-SRS spectra of the different carotenoids are dominated by non-Raman background which closely resembles the temporal cross-correlation of the pump and Stokes as measured by sum-frequency generation (SFG) (black) at the focus of the microscope. There is limited chemical-specific contrast in AM-SRS of such samples. Comparing these AM-SRS spectra to the CM-SRS spectrum (Fig. 4(c) of the main text) or the deconvolved CM-SRS spectrum (Fig. S4(c)) of the same sample, we see that

CM-SRS permits chemical-specific identification and image segmentation, even with very large non-Raman background contributions.

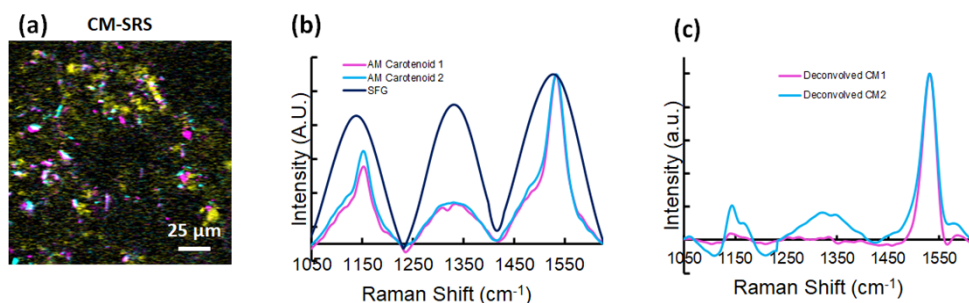


Fig. S4: Sweet potato spectra (a) CM-SRS image of sweet potato. Yellow is recorded at 2850 cm^{-1} , cyan at 1150 cm^{-1} , and magenta at 1520 cm^{-1} after masking out pixels identified in cyan. This is identical to Fig. 4(b) in the main text. (b) AM-SRS spectra of the regions identified using CM-SRS. Magenta and cyan lines are the average spectra measured over all correspondingly colored pixels in (a). For comparison an independently measured SFG response (black line) is included. (c) The spectra recovered when the CM-SRS spectra in Fig. 4(c) are deconvolved.

Strongly absorbing, colored plant materials present further challenges to traditional AM-SRS imaging. As illustrated by the indistinguishability of Figs. 5(a)-(c) in the main text, pine stem is just such a case. Using the CM-SRS images presented in Figs. 5(e)-(g), we can again apply a threshold to define masks (Fig. S5) and record the average CM-SRS spectra for those areas (Figs. S6(a), S6(b)). These can be deconvolved to yield the background-free-equivalent AM-SRS spectra shown in Fig. S6(c). As shown in Fig. S7, much like in sweet potato, in pine stem the AM-SRS spectra (green, red, blue) from the same masked areas are largely similar and closely resemble the cross-correlation measured using sum frequency generation (black). This once again demonstrates the chemical-specific imaging power of CM-SRS, even in strongly absorbing samples where AM-SRS fails. It should be noted that deconvolution procedures are in general susceptible to noise and under sampling, which can lead to a reduction in spectral resolution, apparent in the comparison of Fig. S6(b) with S6(c). However, for the purposes of chemical-specific segmentation/classification and identification of known materials, this is not a limitation as the raw CM-SRS spectra (green, red, blue spectral responses of Fig. S6(b)) can themselves be used directly for image segmentation/classification.

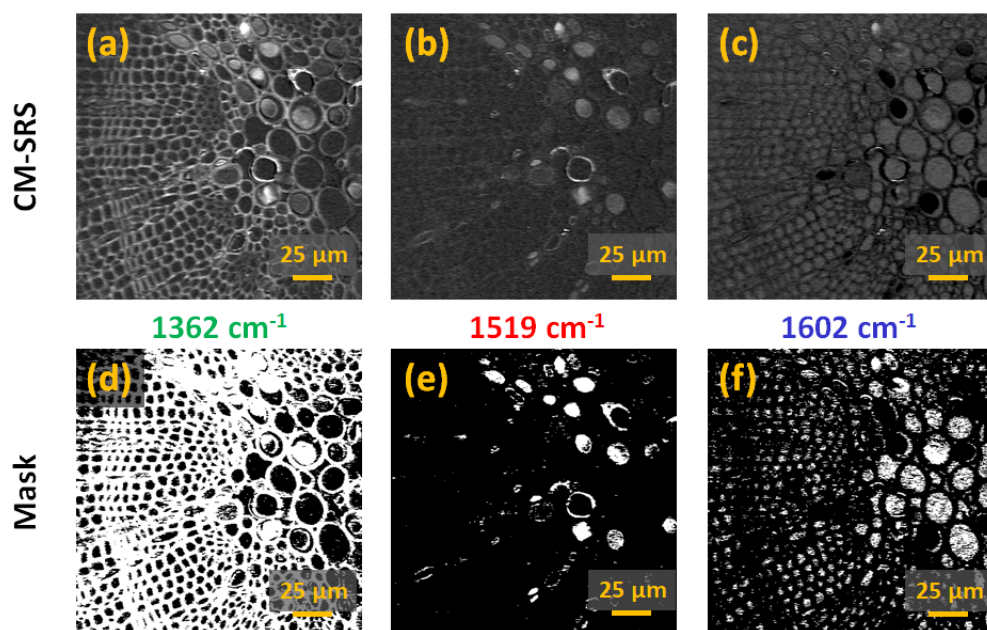


Fig. S5: Masks for segmentation of pine stem. (a) CM-SRS of pine stem recorded at 1362 cm^{-1} . (b) CM-SRS of pine stem recorded at 1519 cm^{-1} . (c) CM-SRS of pine stem recorded at 1602 cm^{-1} . Figs. S4(a)-(c) are identical to Figs. 5(a)-(c) in the main text. For each image, we took a threshold to create a mask to define the area over which the spectrum would be averaged. (d) 1362 cm^{-1} mask. (e) 1519 cm^{-1} mask. (f) 1602 cm^{-1} mask.

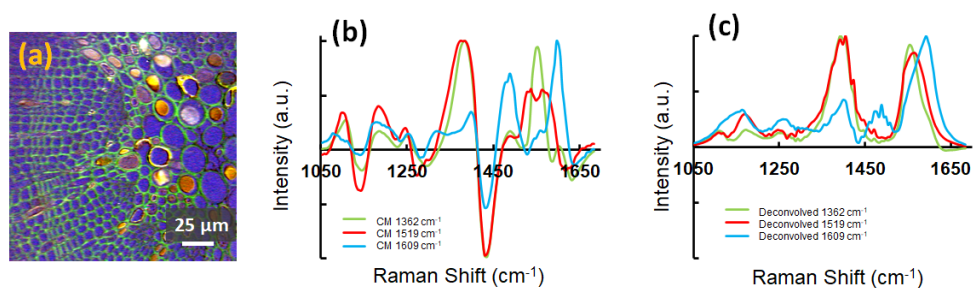


Fig. S6: Pine stem spectra. (a) RGB merge of Figs. 5(e)-(g) in the main text with (e) in green, (f) in red and (g) in blue. This is identical to Fig 5(h) in the main text. (b) CM-SRS spectra averaged over all pixels using masks shown in Figs. S5(d)-(f), green corresponds to mask Fig. S5(d), red to mask Fig. S5(e), and blue to mask Fig. S5(f). (c) The spectra recovered when the CM-SRS spectra in (b) are deconvolved.

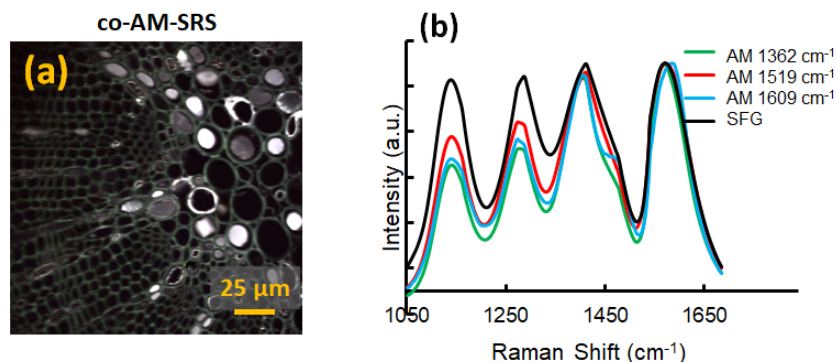


Fig. S7: AM-SRS of pine stem. (a) RGB merge of Figs. 5(a)-(c) in the main text with 5(a) in green, 5(b) in red and 5(c) in blue. The image looks like a grey-scale image because all colours are present with nearly identical intensities in all pixels. This is identical to Fig. 5(d) of in the main text. (b) AM-SRS spectra averaged over all pixels using masks shown in Figs. S5(d)-(f), green corresponds to mask Fig. S5(d), red to mask Fig. S5(e), and blue to mask Fig. S5(f). For comparison, an independently measured SFG spectrum is included (black line).

In order to investigate the small-signal imaging capabilities of CM-SRS, we demonstrated single cell pharmacokinetics of a Raman-labelled (here, CN stretch at 2290 cm^{-1}) small molecule cryo-preservative drug. In Fig. 6 in the main text, we demonstrated monitoring the influx of this small molecule into living cells over the course of several hours. The AM-SRS (black) and CM-SRS spectra (green) of the drug-loaded media are shown in Fig. S8(a): both spectra are centered at 2290 cm^{-1} , the peak of interest for the Raman-labelled molecule. The CM-SRS spectrum has a clear, sharp peak present only in drug-loaded media. However, in this small signal limit where background terms dominate, the AM-SRS spectrum appears as a cross-correlation and is independent of the presence of the drug of interest. In the main text, illustrated in Fig. 6, CM-SRS (tuned to 2290 cm^{-1}) clearly tracked the penetration of the drug into cells, with the average signal strength corresponding to the local drug concentration. We note that, in Fig. 6 of the main text, only one representative image from the four-hour time point was shown. Here we show additional representative images from the one-, two- and five-hour time points in Figs. S8(b)-(d).

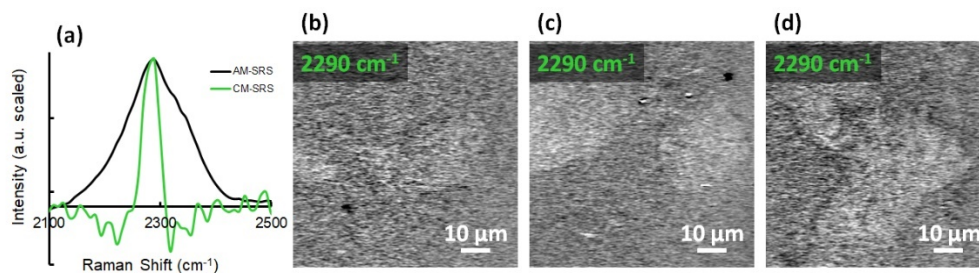


Fig. S8: Ice recrystallization inhibitor (IRI). (a) AM-SRS (black line) and CM-SRS (green line) spectra recorded in IRI loaded media. The AM-SRS response is dominated by non-Raman signals whereas the CM-SRS response has a single isolated peak attributable to a cyano stretch. (b) CM-SRS image of HepG2 cells recorded at 2290 cm^{-1} . This image was recorded 1 hour post IRI exposure and media rinse. (c) CM-SRS image of HepG2 cells recorded at 2290 cm^{-1} . This image was recorded 2 hours post IRI exposure and media rinse. (d) CM-SRS image of HepG2 cells recorded at 2290 cm^{-1} . This image was recorded 5 hour post IRI exposure and media rinse. For the image 4 hours post IRI exposure and media rinse, see the Fig. 6(b) in the main text.

References

1. J. S. Gomez, "Coherent Raman Spectroscopy," in *Modern Techniques in Raman Spectroscopy* (John Wiley & Sons, 1996), pp. 305–342.

2. J. Cheng, A. Volkmer, L. D. Book, and X. S. Xie, "An Epi-Detected Coherent Anti-Stokes Raman Scattering (E-CARS) Microscope with High Spectral Resolution and High Sensitivity," *J. Phys. Chem. B* **105**, 1277–1280 (2001).
3. A. F. Pegoraro, A. Ridsdale, D. J. Moffatt, Y. Jia, J. P. Pezacki, and A. Stolow, "Optimally chirped multimodal CARS microscopy based on a single Ti:sapphire oscillator," *Opt. Express*, OE **17**, 2984–2996 (2009).
4. F. Ganikhanov, C. L. Evans, B. G. Saar, and X. S. Xie, "High-sensitivity vibrational imaging with frequency modulation coherent anti-Stokes Raman scattering (FM CARS) microscopy," *Opt. Lett.*, OL **31**, 1872–1874 (2006).
5. Y. Liu, Y. J. Lee, and M. T. Cicerone, "Broadband CARS spectral phase retrieval using a time-domain Kramers–Kronig transform," *Opt. Lett.*, OL **34**, 1363–1365 (2009).
6. C. H. Camp, "Raman signal extraction from CARS spectra using a learned-matrix representation of the discrete Hilbert transform," *Opt. Express*, OE **30**, 26057–26071 (2022).
7. M. Mohseni, C. Polzer, and T. Hellerer, "Resolution of spectral focusing in coherent Raman imaging," *Opt. Express*, OE **26**, 10230–10241 (2018).
8. M. M. Carrabba, "Wavenumber Standards for Raman Spectrometry," in *Handbook of Vibrational Spectroscopy* (John Wiley & Sons, Ltd, 2006).